Quantum reactive scattering in three dimensions using hyperspherical (APH) coordinates: Periodic Distributed Approximating Functions (PDAF) method for surface functions

Keming Zhang, Gregory A. Parker[*],
Department of Physics and Astronomy
University of Oklahoma, Norman, OK 73019
Donald J. Kouri[†],
Department of Chemistry and Department of Physics
University of Houston, Houston, TX 77204-5641
David K. Hoffman[‡],
Department of Chemistry and Ames Laboratory,
Iowa State University, Ames, IA 50011
and
Srinivasan S. Iyengar
The Henry Eyring Center for Theoretical Chemistry and Department of Chemistry
The University of Utah, Salt Lake City, UT 84112

January 30, 2002

Periodic distributed approximating functions (PDAFs) are proposed and used to obtain a coordinate representation for the Adiabatically Adjusting Principal Axis Hyperphysical (APH) coordinates kinetic energy operator. The approach is tested and accurate results for adiabatic surface functions of reaction $F+H_2 \rightarrow HF+H$ are calculated and compared to those of some existing methods.

1 Introduction

In hyperspheical coordinate formulations of reactive scattering, the total wave function is expanded in Wigner rotaion functions of three Euler angles describing the spatial orientation of the plane formed by the three particles and basis functions of two internal hyperspherical angles, and then the dependece of the hyperradius, ρ , is determined by propagating the set of coupled channel(CC) differential equations from small ρ, where the solutions must be regular, to large ρ where they can be projected onto the arrangement channels to determine the scattering matrix. In the methods using those hyperspherical coordinates which treat all of the particles symmetrically[1, 2, 3, 4, 5, 6, 7, 8], one obtains "surface functions," the basis functions of the two hyperangles which cover the surface of the internal coordinate sphere or "hypershphere," by solving a two dimensional (2D) Schrödinger equation. This equation, which is discussed in more detail later in this paper, depends parametrically on ρ and must be solved at many values of ρ. In adddition, a large number of these surface functions must be obtained at each ρ, so that it is important to have an efficient method for finding them.

[*]Supported under National Science Foundation Grant CHE-9710383 and PHY-0100704.
[†]Supported under National Science Foundation Grant CHE-9700297.
[‡]The Ames Laboratory is supported by the Department of Energy under Contract No 2-7405-ENG82

The first accurate 3D reactive scattering calculations using hyperspherical coordinates used finite element methods (FEMs)[3, 4, 5, 9, 8, 10, 11] to solve the surface function equation. Although these FEMs give fairly accurate results, they work inefficient and are not robust. Another typical method in calculations on several reactions is the discrete variable representation (DVR)[5, 6, 14, 15, 16]. DVR is most efficient at small ρ where the surface functions are delocalized, however at large ρ, where the surface function are highly localized, the DVR points still cover the whole space, thus it becomes much less efficient. In a few cases the DVR is even more expensive than the FEM because of the need for many grid points in a small, localized region. Other methods such as the finite basis representation (FBR)[1, 2, 7] of Launay and LeDourneuf, and the method of Wolniewicz and Hinze[29] are also efficient only at large ρ. Analytic basis method (ABM) uses primitive basis functions centered in the arrangement channels, it gives very compact representation and thus very efficient at large ρ, but it is inefficient and tends to diverge at small ρ.

In this paper, we will present a Peridoical Distributed Approximating Function (PDAF) method, which work very efficiently at both small ρ and large ρ. The PDAF method is similar to the method of Iyengar and Parker's method[12], but in their method, they solve the 3D wavefunctions by diagonilzing a large real non-symmetric matrices, which is practical only for identical-atom system. Our new method solves only the surface functions, and we transform the Hamiltonian matrix into real symmetric matrices. Similarly but in a simpler way, we make the Hamitonian symmetry-adaptive, thus increses the efficiency of the computation. We employ the Distributed Approximating Function (DAF) concept, but we do not use any existed DAF formula, on the other hand, we proposed the PDAF directly, which turns out to be more accurate and efficient. The sequential diagonalization-truncation technique[13] is employed to project the large-size Hamiltonian matrix into a smaller matrix using a projection matrix which is obtained by solving an one-dimensional eigensystem, thus significantly reduce the memory requirement and the computation time.

This paper is organized as follows. In Sec. 2 we introduce the PDAFs and derive their formulae. In Sec. 3 the ro-vibrational triatomic Hamiltonian in the APH coordinates system is presented and the symmetrization and reductions of the Hamiltonian are illustrated. The PDAF approach is then tested in Sec. 4 . The surface functions of FH_2 scattering are computed, and the eigen-energies and the matrix elements are calculated and compared to those of the existed methods(FEM, ABM and DVR) in Sec. 5 . Sec. 6 makes a conclusion of this paper.

2 Periodic Distributed Approximating Function (PDAF)

sec:PDAF

From the definition of the Dirac Delta function we know that

$$f(x) = \int_{-\infty}^{\infty} \delta(x - x') f(x') dx' \tag{1}$$

for any continuous function $f(x)$.

Now we condsider periodic functions, $f_p(x)$, with period 2π. The present method can be trivally extended to periodic functions with an arbitrary period. With this assumption the equations are slightly simpler and easier to interpret. Expressing the integration range as an infinite sum of segments of length 2π we can write

$$f_p(x) = \sum_{m=-\infty}^{\infty} \int_0^{2\pi} \delta(x - x' - 2m\pi) f_p(x' + 2m\pi) dx'. \tag{2}$$

Interchanging the integral and sum then using the periodicity of $f_p(x)$, we have

$$f_p(x) = \int_0^{2\pi} \sum_{m=-\infty}^{\infty} \delta(x - x' - 2m\pi) f_p(x') dx' \tag{3}$$

or

$$f_p(x) = \int_0^{2\pi} \delta_p(x - x') f_p(x') dx' \tag{4}$$

eq:PDAFint0

where

$$\delta_p(x-x') = \sum_{m=-\infty}^{\infty} \delta(x-x'-2m\pi) \tag{5}$$

is the periodic delta function. Since $\delta(x)$ is an even function, it's easy to see that $\delta_p(x)$ is even and is also periodic with a period of 2π. Taking the k^{th} derivative of $f_p(x)$, we have,

$$f_p^{(k)}(x) = \int_0^{2\pi} \delta_p^{(k)}(x-x') f_p(x') dx'. \tag{6}$$ eq:PDAFint

Now expand both $f_p(x)$ and $\delta_p(x-x')$ in a fourier series

$$\delta_p(x-x') = \frac{a_0}{2} + \sum_{n=1}^{\infty} a_n \cos n(x-x') \tag{7}$$

$$f_p(x) = \frac{b_0}{2} + \sum_{n=1}^{\infty} b_n \cos nx + c_n \sin nx. \tag{8}$$

Substituting $f_p(x)$ and $\delta_p(x-x')$ into (4) and using the following identities

$$\int_0^{2\pi} \cos[m(x-x')]\cos(nx')dx' = \begin{cases} \delta_{mn}\pi\cos nx & n \neq 0 \\ \delta_{mn}2\pi & n=0 \end{cases} \tag{9}$$

$$\int_0^{2\pi} \cos[m(x-x')]\sin nx' dx' = \delta_{mn}\pi \sin nx \tag{10}$$

we obtain expressions for the expansion coefficients

$$a_0 = a_n = \frac{1}{\pi}, \qquad n = 1, 2, \ldots \tag{11}$$

Thus we get the formula for the periodic delta function,

$$\delta_p(x-x') = \frac{1}{\pi}\left(\frac{1}{2} + \sum_{n=1}^{\infty} \cos n(x-x')\right). \tag{12}$$ eq:PDAFexact

The partial sum of the periodic delta function is the continuous Periodic Distributed Approximating Function (PDAF)

$$\delta_{p,M}(x-x') = \frac{1}{\pi}\left[\frac{1}{2} + \sum_{n=1}^{M} \cos n(x-x')\right] \tag{13}$$ eq:PDAF

which is the final formula used in this work. We also note that as M increases the PDAF approaches the periodic delta function, i.e.

$$\delta_p(x-x') = \lim_{M\to\infty} \delta_{p,M}(x-x'). \tag{14}$$

One may obtain the fully discretized PDAF by approximating the integral over x' in (6) using a trapezoidal quadrature

$$f_{p,M}^{(k)}(x_i) = \sum_{j=1}^{N} \delta_{p,M}^{(k)}(x_i - x_j) f_p(x_j) \Delta x \tag{15}$$ eq:PDAFintd

where N is the number of grid points, $\Delta x = \frac{2\pi}{N}$ and $x_j = (j - \frac{1}{2})\Delta x$. Note the coordinate x was also discretized using the same grid points as used in the numerical quadrature. This choice of quadrature points is particularly useful if we are solving differential equations with singular points at the two ends ($x = 0$ and $x = 2\pi$). As the grid points are fixed, $\delta^{(k)}_{p,M}(x)$ acts like the k^{th} derivative operator. If we treat $f_{p,M}(x)$ as a column vector $[f_j = f(x_j)]$, we have

$$f^{(k)}_{i,M} = \sum_{i=1}^{N} D^{(k)}_{ij} f_j \tag{16}$$

where

$$D^{(k)}_{ij} = \delta^{(k)}_{p,M}(x_i - x_j)\Delta x \tag{17}$$ eq:D

is the k^{th} derivative operator in matrix form. The differential operators, $D^{(k)}$ are periodic Toeplitz matrices independent of the periodic function $f_p(x)$, and depend on only one parameter M. The column vector $f^{(k)}_{i,M}$ is the PDAF approximate to the k^{th} derivitive of $f_p(x)$, i.e.

$$f^{(k)}_{i,M} \approx \frac{d^k}{dx^k} f_p(x)\Big|_{x=x_i}. \tag{18}$$

For large M the PDAF is a more accurate representation of the Dirac delta function. However, for small M the integrand of (6) is smoother and the trapezoidal rule is more accurate. Hence, there is an optimal value of M which is chosen to make the agreement as close as possible. Through numerical experimentation (see Sec. 4) we found that $M = N/2$, gives the most accurate results, where N is the number of grid points in the 2π range. In this paper, we will use $D^{(0)}$, $D^{(1)}$ and $D^{(2)}$, consequently we need $\delta^{(0)}_{p,M}$, $\delta^{(1)}_{p,M}$ and $\delta^{(2)}_{p,M}$. They can be obtained by simply differentiating (13). The general results for any k are,

$$\delta^{(k)}_{p,M}(x) = \begin{cases} (-1)^{\frac{k+1}{2}} \frac{1}{\pi} \sum_{n=1}^{M} n^k \sin nx & k \text{ odd} \\ \\ \frac{1}{2\pi}\delta_{0,k} + (-1)^{\frac{k}{2}} \frac{1}{\pi} \sum_{n=1}^{M} n^k \cos nx & k \text{ even} \end{cases} \tag{19}$$

We see that $\delta^{(k)}_{p,M}(x)$ are even(odd) periodic functions when k is even(odd). The functions, $\delta^{(0)}_{p,M}(x)$, $\delta^{(1)}_{p,M}(x)$, and $\delta^{(2)}_{p,M}(x)$ are shown in Fig. 1 . In both panels of Fig. 1 $N = 20$, in the left panel $M = 5$ and in the right panel $M = N/2 = 10$. One can readily see the symmetry of each PDAF. Comparing the left and right panels in Fig. 1 we see that increasing M makes the PDAFs in the right panel sharply peaked and a better representation of the respective Dirac Delta function and its derivatives.

3 Symmetrization and Reductions of the Triatomic Hamiltonian in APH Coordinates

3.1 APH Hamiltonian

The detailed reactive scattering theory formulated in adiabatically adjusting principle axes hyperspherical (APH) coordinates has been presented previously[3], and we repeat only the essentials here. In this approach, one needs sector adiabatic basis functions $\Phi^p_{\tau\Lambda}$ of the APH hyperangles, and in this work we choose $\Phi^p_{\tau\Lambda}$ to satisfy the equation

$$H\Phi^p_{\tau\Lambda}(\theta, \chi; \rho_\xi) = \mathcal{E}^p_{\tau\Lambda}(\rho_\xi)\Phi^p_{\tau\Lambda}(\theta, \chi; \rho_\xi) \tag{20}$$ eq:Schrodinger

where

$$H = -\frac{\hbar^2}{2\mu\rho_\xi^2}\left[\frac{4}{\sin 2\theta}\frac{\partial}{\partial\theta}\sin 2\theta\frac{\partial}{\partial\theta} + \frac{1}{\sin^2\theta}\frac{\partial^2}{\partial\chi^2}\right] + \frac{15\hbar^2}{8\mu\rho_\xi^2} + C\hbar^2\Lambda^2 + V(\rho_\xi, \theta, \chi) \tag{21}$$ eq:H

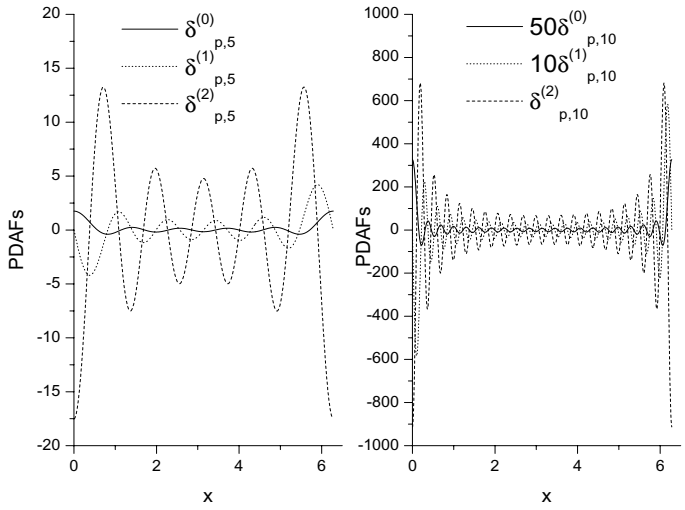

Figure 1: $\delta^{(k)}_{p,M}(x)$ for different M, where the number of grid points ($N = 20$) is used in both panels. In the left panel $M = 5$ and in the left panel and $M = N/2 = 10$. Note $\delta^{(0)}_{p,M}$ and $\delta^{(2)}_{p,M}$ are symmetric about $x = 0$, while $\delta^{(1)}_{p,M}$ is anti-symmetric. Increasing M makes the PDAFs sharply peaked and a better representation of the respective delta function and its derivatives.

fig:PDAFs

The first term in the Hamiltonian H is the "hyperspherical" part of the kinetic energy operator, and

$$C = \frac{1}{\mu\rho_\xi^2(1-\sin\theta)} \tag{22}$$

is part of the centrifugal potential. The potential energy V used here is the whole potential energy surface (PES) of Brown et al.[18], and the $\mathcal{E}^p_{\tau,\Lambda}$ are the eigenenergies. The variable θ is the APH bending angle; its range is $0 \le \theta \le \pi/2$, with $\pi/2$ describing linear configurations and 0 describing triangular symmetric top configurations. χ is the APH kinematic angle measured from the "incident" arrangement channel; it measures motion between arrangement channels, and its range is $-\pi \le \chi \le \pi$. The angles θ and χ cover the upper half of the surface of an internal coordinate sphere which we loosely call the "hypersphere". (More precisley, the surface of the hypersphere is the 5D space covered by θ, χ, and the three Euler angles which describe the orientation of the principal axes in space.) As one can see from (20), the surface functions $\Phi^p_{\tau,\Lambda}$ and eigenenergies $\mathcal{E}^p_{\tau,\Lambda}$ depend parametrically on the hyperradius ρ_ξ. They are needed at a set of ρ values $\{\rho_\xi\}, \xi = 1, 2, ..., n_\rho$, which are used as adiabatic basis functions for expanding the full wavefunction in each sector where $\rho \in [(\rho_\xi + \rho_{\xi-1})/2, (\rho_{\xi+1} + \rho_\xi)/2]$ for sector ξ. As shown elsewhere[3] this adiabatic-by-sector (or sector Adiabatic) wavefunction gives rise to a set of coupled second order differential equations. These Coupled-Channel (CC) equations must be numerically integrated from a small value of the hyperradius ρ where the full wavefunction is zero to a large value of the hyperradius where asymptotic boundary conditions are applied. The $15\hbar^2/8\mu\rho^2$ term in (21) comes from removal of first derivative terms from the coupled channel (CC) equations; it is a constant in this equation and can be folded into the $\mathcal{E}^p_{\tau,\Lambda}$ if desired. In the numerical calculations we used atomic units throughout and therefor Planck's constant divided by 2π, $\hbar = 1$. μ is the three-body reduced mass of the system arising from mass-scaled coordinates. The three quantum numbers (Λ, p, τ) labeling $\mathcal{E}^p_{\tau,\Lambda}$ and $\Phi^p_{\tau,\Lambda}$ are: Λ the component of the total angular momentum along the APH body-frame (BF) z-axis (the axis of least inertia of the three-body system), p the parity quantum number with $p = 0$ or 1, the parity of $\Phi^p_{\tau,\Lambda}$ under the parity transformation $\chi \to \chi \pm \pi$ is $(-1)^p$, and $\tau = 1, 2, ..., n_\Phi$, which indexes the solutions in order of increasing energy.

We note that (21) differs from equation (164) of Reference[3] slightly because it omits a rotational term of the form $\frac{1}{2}(A+B)\hbar^2[J(J+1)-\Lambda^2]$. As pointed out by Launay and LeDourneuf [1], this omission gives surface functions $\Phi^p_{\tau,\Lambda}$ which are independent of the total angular momentum J, so many fewer surface functions must be calculated. The omitted term is easily included in the CC equations along with the remaining Coriolis and asymmetric top terms. This surface function basis is expected to produce rapid convergence of the CC expansion to the exact solution provided triangular symmetric top ($\theta = 0$) configurations are unimportant, which is the case for many reactions.

The full wavefunction must be continuous and regular everywhere. This requires that $\Phi^p_{\tau,\Lambda}$ must be a continuous function of χ at $-\pi$ and π and regular everywhere. For systems with two or three identical atoms, the surface functions have other symmetries in addition to the parity p already defined and these symmetries will be incorporated. The surface functions are real and normalized according to

$$\int_{-\pi}^{\pi} d\chi \int_0^{\pi/2} \Phi^{p^\emptyset}_{\tau^\emptyset\Lambda}(\theta,\chi;\rho_\xi)\Phi^p_{\tau\Lambda}(\theta,\chi;\rho_\xi)\sin 2\theta d\theta = \delta_{\tau^\emptyset\tau}\delta_{p^\emptyset p}. \tag{23}$$ eq:norm

We will use the PDAFs to solve the time-independent Schrödinger (20). To make it easier to discuss, we define the following terms:

$$H_\theta = -\frac{4}{\sin 2\theta}\frac{\partial}{\partial\theta}\sin 2\theta\frac{\partial}{\partial\theta} \tag{24}$$

$$H_\chi = -\frac{\partial^2}{\partial\chi^2} \tag{25}$$

$$H_V = \frac{15\hbar^2}{8\mu\rho_\xi^2} + C\hbar^2\Lambda^2 + V(\rho_\xi,\theta,\chi). \tag{26}$$

With these definitions the surface function Hamiltonian, (21), is

$$H = \frac{\hbar^2}{2\mu\rho_\xi^2}\left[H_\theta + \frac{1}{\sin^2\theta}H_\chi\right] + H_V. \tag{27}$$ eq:Hsimp

Since a discretized Hamiltonian is a matrix operator, we can simply treat it as a matrix. In the rest of this paper, A Hamiltonian and a matrix will be used interchangeably. For example, when we say that H_χ is symmetric, that means the the matrix of discretized H_χ is a symmetric matrix.

3.2 Symmetrization of APH Hamiltonian

sub:symAPH

The Hamiltonian H in (27) is real but it is not symmetric, because H_θ is not symmetric. So if we just use this form, we have to solve a complex matrix eigensystem. A large amount of memory and increased CPU time is required to solve large nonsymmetric eigensystems. Since both memory and CPU time are critical in the computation of APH surface functions, we need symmetrize H. H_θ is the essentially non-symmetric part of H, and it is not periodic. So we first extend H_θ to a periodic form and symmetrize it. Then the result is extended to symmetrize H.

One might have noted that H_θ is not periodic because $0 \le \theta \le \frac{\pi}{2}$, but it can be easily extended to a periodic form. Suppose H_θ satisfies the following eigensystem,

$$H_\theta\psi(\theta) = \lambda\psi(\theta) \tag{28}$$ eq:eigen-theta

The solution $\psi(\theta)$ must be regular everywhere, which leads to the the boundary condition,

$$\left.\frac{d\psi}{d\theta}\right|_{\theta=0} = \left.\frac{d\psi}{d\theta}\right|_{\theta=\frac{\pi}{2}} = 0 \tag{29}$$

so we can extend the domain of $\psi(\theta)$ to the full real space by defining,

$$\begin{aligned} \psi(\theta) &= \psi(\pi-\theta), \quad \frac{\pi}{2} \le \theta \le \pi & (30) \\ \psi(\theta+k\pi) &= \psi(\theta), \quad 0 \le \theta \le \pi \text{ and } k = 0, \pm 1, \pm 2, ... & (31) \end{aligned}$$

Now $\psi(\theta)$ is a periodic function with a periodicity of π. Note that

$$\begin{aligned} H_\theta(\theta) &= H(\pi-\theta) & (32) \\ H_\theta(\theta+k\pi) &= H(\theta), \quad k = 0, \pm 1, \pm 2, ... & (33) \end{aligned}$$

One can see that the extended $\psi(\theta)$ satisfies (28) for any θ, i.e. the domain of H_θ is also extended to the full real space although it keeps its original form.

To get the symmetric H_θ, we transform it in two steps. First we introduce a continuous mapping function,

$$\theta(\gamma) = \frac{\pi}{4}(1 - \cos(\gamma + 2k\pi)) - k\pi, \quad k = 0, \pm 1, \pm 2, ... \tag{34}$$

We note that the first derivative of this mapping is also continuous, but its second derivative is discontinuous at $\theta = k\pi/2$. This problem is handled by the mapping function itself: we use a uniform grid scheme for γ, it is equivalent that we use a non-uniform grid scheme for θ which is dense near the singularities ($\theta = k\pi/2$) and sparse otherwise, as shown in Fig. 2 . Since more grid points are used in the $\theta = k\pi/2$ region, high accuracy can be obtained despite the discontinuity.

Substituting θ with γ in (24), we obtain,

$$H_\theta(\gamma) = -\frac{64}{\pi^2}\frac{1}{\sin 2\theta(\gamma)\sin\gamma}\frac{\partial}{\partial\gamma}\frac{\sin 2\theta(\gamma)}{\sin\gamma}\frac{\partial}{\partial\gamma} \tag{35}$$

$H_\theta(\gamma)$ is very similar to $H_\theta(\theta)$ except that it has a periodicity of 2π.

In the second step, we define transformation function

$$T = \sqrt{\sin 2\theta \sin\gamma} \tag{36}$$

We also need

$$\begin{aligned} T^\dagger &= T & (37) \\ T^{-1} &= \frac{1}{\sqrt{\sin 2\theta \sin\gamma}} & (38) \end{aligned}$$

and it is important to note that the singularities in this inversion are avoided by our choice of quadrature (see Sec. 2). Applying $T^\dagger$ to the (28) and insert identity $T^{-1}T$ between H_θ and $\psi(\theta)$, we obtain

$$H_\gamma T\psi(\theta) = \lambda T\psi(\theta) \tag{39}$$

eq:SymThetaEigenEqua

where

$$\begin{aligned} H_\gamma &= T^\dagger H_\theta(\gamma) T^{-1} \\ &= -\frac{64}{\pi^2}\frac{1}{\sqrt{\sin 2\theta(\gamma)\sin\gamma}}\frac{\partial}{\partial\gamma}\frac{\sin 2\theta(\gamma)}{\sin\gamma}\frac{\partial}{\partial\gamma}\frac{1}{\sqrt{\sin 2\theta(\gamma)\sin\gamma}} & (40) \end{aligned}$$

is a symmetric Hamiltonian.

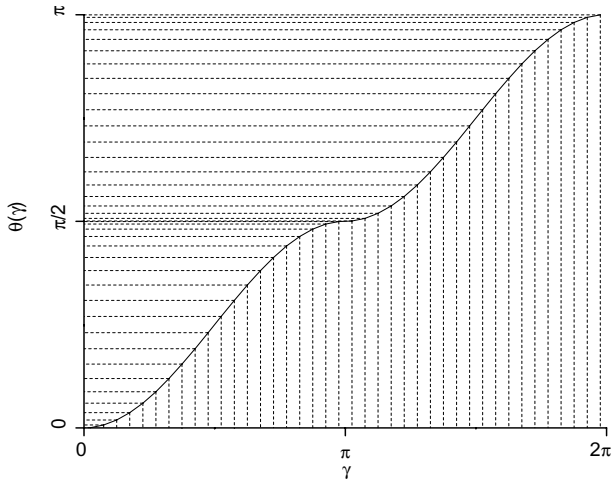

Figure 2: Grid mapping function $\theta(\gamma)$. The uniform grid scheme in θ corresponds to the non-uniform grid scheme for θ which is dense near the singularities($\theta = k\pi/2$) and sparse otherwise. fig:theta-gamma

The eigenfunction of H_γ is

$$\tilde{\psi}(\gamma) = T(\gamma)\psi(\theta(\gamma)) \tag{41}$$ eq:psitilde

which is always zero at $\gamma = 0, \pi$, or 2π. It is not hard to see that extending $\psi(\theta)$ from $0 \le \theta \le \frac{\pi}{2}$ to $0 \le \theta \le \pi$ introduces undesired degenerate eigenvalues. If we reduce matrix H_γ from $0 \le \theta \le 2\pi$ to range $0 \le \theta \le \pi$ using the symmetry of ψ, we can eliminate those undesired degenerate eigenvalues. We use a grid scheme similar to the one for PDAF, say,

$$\gamma_j = (j - \frac{1}{2})\Delta\gamma, \quad j = 1, 2N_\gamma \tag{42}$$

where $2N_\gamma$ is the number of gird points, and $\Delta\gamma = \frac{2\pi}{2N_\gamma} = \frac{\pi}{N_\gamma}$ is the distance between two consecutive grid points. For simplicity, we use a subscript j to denote a term evaluated at γ_j, and we also define the following terms,

$$t_j = \frac{1}{\sqrt{\sin 2\theta(\gamma_j) \sin \gamma_j}} \tag{43}$$

$$s_j = \frac{\sin 2\theta(\gamma_j)}{\sin \gamma_j} \tag{44}$$

Applying the derivative operator $D^{(1)}$ in (17) (substitute x with γ), the eigen-equation (39) can be

written as,

$$\begin{aligned}
\lambda\tilde{\psi}_i &= \sum_{j=1}^{2N}\sum_{k=1}^{2N} -\frac{64}{\pi^2} t_i D^{(1)}_{ik} s_k D^{(1)}_{kj} t_j \tilde{\psi}_j \\
&= (\sum_{j=1}^{N} + \sum_{j=N+1}^{2N}) \sum_{k=1}^{2N} -\frac{64}{\pi^2} t_i D^{(1)}_{ik} s_k D^{(1)}_{kj} t_j \tilde{\psi}_j \\
&= \sum_{j=1}^{N}\sum_{k=1}^{2N} -\frac{64}{\pi^2} t_i D^{(1)}_{ik} s_k (D^{(1)}_{kj} + D^{(1)}_{k\,2N-j+1}) t_j \tilde{\psi}_j \\
&= \sum_{j=1}^{N} H^r_{\gamma_{ij}} \tilde{\psi}_j \qquad (45)
\end{aligned}$$

where

$$H^r_{\gamma_{ij}} = \sum_{k=1}^{2N} -\frac{64}{\pi^2} t_i D^{(1)}_{ik} s_k (D^{(1)}_{kj} + D^{(1)}_{k\,2N-j+1}) t_j \qquad (46)$$

eq:Hrgamma

In the above derivation, $\tilde{\psi}_j = \tilde{\psi}_{2N-j+1}$, $t_j = t_{2N-j+1}$, $s_j = s_{2N-j+1}$ and the periodicity of $D^{(1)}$ are applied. One should note that in (45) $1 \le i \le N_\gamma$ and $1 \le i \le N_\gamma$, which means $0 \le \gamma \le \pi$, so H^r_γ is reduced to the original domain. H^r_γ is the desired form for H_θ and it is easy to show that H^r_γ is a symmetric matrix.

Similarly we can transform and discretize H to get the symmetric form of H. Using (27) the Schrödinger (20) reads,

$$\left\{ \frac{\hbar^2}{2\mu\rho_\xi^2} \left[H_\theta + \frac{1}{\sin^2\theta} H_\chi \right] + H_V \right\} \Phi^p_{\tau\Lambda}(\theta,\chi;\rho_\xi) = \mathcal{E}^p_{\tau\Lambda}(\rho_\xi) \Phi^p_{\tau\Lambda}(\theta,\chi;\rho_\xi) \qquad (47)$$

Left multiply $T^\dagger$ to both sides of the above equation and insert identity $T^{-1}T$, we obtain

$$H^s \overline{\Phi}^p_{\tau\Lambda}(\theta,\chi;\rho_\xi) = \mathcal{E}^p_{\tau\Lambda}(\rho_\xi) \overline{\Phi}^p_{\tau\Lambda}(\theta,\chi;\rho_\xi) \qquad (48)$$

eq:sym-Schrodinger

where

$$H^s = \frac{\hbar^2}{2\mu\rho_\xi^2} \left[H^r_\gamma + \frac{1}{\sin^2\theta} H_\chi \right] + H_V \qquad (49)$$

eq:sym-H

and

$$\overline{\Phi}^p_{\tau\Lambda}(\gamma,\chi;\rho_\xi) = T \Phi^p_{\tau\Lambda}(\theta,\chi;\rho_\xi) \qquad (50)$$

The independency of γ(or θ) and χ is used in the derivation. After discretization, H^s is symmetric, because H^r_γ is symmetric, H_V is diagonal, and H_χ is obviously symmetric. Thus we obtain the symmetric form of APH Hamiltonian, H^s.

3.3 Reduction of the H_χ using symmetry

If the Hamiltonian H^s of a system commutes with a point group G, i.e. the potential H_V is symmetric under the operations of G, we can reduce the size of the Hamiltonian matrix by transform the Hamiltonian into the irreducible representations of the G.

Let $G = \{R\}$, where $\{R\}$ is a set of symmetry operations such as rotations and reflections. The order of G is h, i.e, G contains h symmetry operations, R. Suppose H_χ satisfies the following eigen-equation,

$$H_\chi \phi^{[z,\kappa]}(\chi) = \lambda \phi^{[z,\kappa]}(\chi) \qquad (51)$$

eq:eigen-Hchi

where $\phi^{[z,\kappa]}$ transform according the κ-th column of the z-th irreducible representation of G, i.e. $\phi^{[z,\kappa]}$ is the κ-th basis function for the τ-th ireducible representation, and λ is the eigenvalue. We will discretize (51) using a uniform grid scheme, say,

$$\chi_j = (j - 1/2)\Delta\chi, \quad j = 1, hN_\chi \tag{52}$$ eq:chischeme

where hN_χ is the number of grid points, $\Delta\chi = \frac{2\pi}{hN_\chi}$ is the distance between two consecutive grid points, and clearly N_χ is the number of grid points in interval $[0, \frac{2\pi}{h}]$. Now (51) can be written as,

$$\sum_{j=1}^{hN_\chi} H_\chi(\chi_i, \chi_j)\phi^{[z,\kappa]}(\chi_j) = \lambda\phi^{[z,\kappa]}(\chi_i), \quad \kappa = 1, l_z \tag{53}$$ eq:discHchi

where l_z is the dimension of the z-th irreducible representation. The the full range of χ can be generated by applying each symmetry operation R on range $[1, N\chi]$, thus we can write (53) as

$$\sum_{j=1}^{N_\chi}\sum_{R} H_\chi(\chi_i, R\chi_j)\phi^{[z,\kappa]}(R\chi_j) = \lambda\phi^{[z,\kappa]}(\chi_i), \quad \kappa = 1, l_z \tag{54}$$ eq:RdiscHchi

From the well-known relations [23],

$$\phi^{[z,\kappa]}(R^{-1}\chi) = \sum_{\kappa^\theta} \phi^{[z,\kappa^\theta]}(\chi)\Gamma^{[j]}_{\kappa^\theta,\kappa}(R) \tag{55}$$ eq:PR-1

where $\Gamma^{[z]}_{\kappa^\theta,\kappa}(R)$ is the (κ', κ)-th element of the z-th irreducible representation matrix of R, we have,

$$\begin{aligned}
\phi^{[z,\kappa]}(R\chi) &= \sum_{\kappa^\theta} \phi^{[z,\kappa^\theta]}(\chi)\Gamma^{[z]}_{\kappa^\theta,\kappa}(R^{-1}) \\
&= \sum_{\kappa^\theta} \phi^{[z,\kappa^\theta]}(\chi)\Gamma^{[z]\dagger}_{\kappa^\theta,\kappa}(R) \\
&= \sum_{\kappa^\theta} \phi^{[z,\kappa^\theta]}(\chi)\Gamma^{[z]*}_{\kappa,\kappa^\theta}(R)
\end{aligned} \tag{56}$$

The following obvious properties of $\Gamma^{[z]}_{\kappa^\theta,\kappa}(R)$ are used in the above derivation,

$$\Gamma^{[z]}(R^{-1}) = \Gamma^{[z]^\dagger}(R) = \Gamma^{[z]^{-1}}(R) \tag{57}$$ eq:GammaProperty

Plug (56) into (54), we obtain,

$$\sum_{j=1}^{N_\chi}\sum_{R} H_\chi(\chi_i, R\chi_j)\sum_{\kappa^\theta} \phi^{[z,\kappa^\theta]}(\chi_j)\Gamma^{[j]*}_{\kappa,\kappa^\theta}(R) = \lambda\phi^{[z,\kappa]}(\chi_i), \quad \kappa = 1, l_z \tag{58}$$ eq:red-Hchi

(58) is a set of coupled equations. It would be concise if we write it in a matrix form. For triatomic reactions, the relevant irreducible representations are either one-dimensional or two-dimensional. For the one-dimensional case, $\kappa = \kappa' = 1$, so we simply omit them. Hence we have,

$$\sum_{j=1}^{N_\chi} H^r_\chi(\chi_i, \chi_j)\phi^{[z]}(\chi_j) = \lambda\phi^{[z]}(\chi_i) \tag{59}$$ eq:red-1D-Hchi

where

$$H^r_\chi(\chi_i, \chi_j) = \sum_R H_\chi(\chi_i, R\chi_j)\Gamma^{[z]*}(R) \tag{60}$$ eq:redHchi-1D

is the reduced H_χ in an one-dimensional irreducible representation.

For the two-dimensional case, we have,

$$\sum_{j=1}^{N_\chi} H^r_\chi(\chi_i,\chi_j)\begin{pmatrix}\phi^{[z,1](\chi_j)}\\ \phi^{[z,2](\chi_j)}\end{pmatrix} = \lambda\begin{pmatrix}\phi^{[z,1](\chi_i)}\\ \phi^{[z,2](\chi_i)}\end{pmatrix} \tag{61}$$

eq:red-2D-Hchi

where

$$H^r_\chi(\chi_i,\chi_j) = \sum_R H_\chi(\chi_i, R\chi_j)\Gamma^{[z]*}(R) \tag{62}$$

eq:redHchi-2D

is the reduced H_χ in a two-dimensional irreducible representation. It has the same form as in the one-dimensional case, but it is a 2×2 matrix. H^r_χ can be proved symmetric if the associated irreducible representation matrices are real (see Appendix A). There are three types triatomic interactions:

ABC All atoms are distinct. The point group corresponding to this type is C_2

AAB Two atoms are identical, but the other is different. The point group corresponding to this type is C_{2v}

AAA All atoms are identical. The point group corresponding to this type is C_{6v}

For all the above groups in each type, the irreducible representation matrices are all real, so H^r_χ is symmetric. We provide the representation matrices in Appendix B for reference.

One should note that if we confine χ in $[0, \frac{2\pi}{h}]$, H^r_χ is a $N_\chi \times N_\chi$ matrix in an one-dimensional irreducible representation and a $2N_\chi \times 2N_\chi$ matrix in a two-dimensional irreducible representation. When the eigensystem of (59) or (61) is solved, eigenfunctions of range $[0, \frac{2\pi}{h}]$ is obtained. One can employ (55) to compute the eigenfunctions of the full range of χ.

One can see that using H^r_χ instead of H_χ doesn't affect the symmetrization of H in Sec. 3.2 . Hence we can use the following definition of H^s in the rest of this paper without confusion,

$$H^s = \frac{\hbar^2}{2\mu\rho_\xi^2}\left[H^r_\gamma + \frac{1}{\sin^2\theta}H^r_\chi\right] + H_V \tag{63}$$

eq:sym-H-group

3.4 Reduction of the Hamiltonian using projection

sub:red-prj

Suppose we discretize H^s using N_χ grid points in χ coordinate and N_γ in γ, the size of the Hamiltonian matrix ($N_\gamma N_\chi \times N_\gamma N_\chi$) to be diagonalized is very large for systems of physical interest when highly accurate eigenvalues and eigenfunctions are needed. On the other hand, we need to reduce the CPU time and memory as much as possible. Since we are interested in only a few of the lowest eigenstates, we may waste a lot of time and memory to compute the full eigensystem. To reduce the CPU time and memory allocation the reduction of the Hamiltonian matrix needs to be considered. First we find a nearly complete basis for the desired lowest eigenvectors, and then we project the Hamiltonian matrix to this basis: $H^{\rm cut} = \widetilde{P}H^sP$, where P is the projection matrix and $\widetilde{P}$ is the transpose of P. The size of $H^{\rm cut}$ is small. We solve the eigensystem of $H^{\rm cut}$ and map it back to the original basis to obtain the approximate eigensystem of the H. Details are given below.

Noting H^r_γ depends on only γ and $\frac{\hbar^2}{2\mu\rho_\xi^2}$ is a constant, and introducing the identity matrix I_γ and I_χ in the γ and χ spaces respectively, we can rewrite the Hamiltonian H^s in (63) in the cross product form,

$$H^s = \frac{\hbar^2}{2\mu\rho_\xi^2}H^r_\gamma\otimes I_\chi + (\frac{\hbar^2}{2\mu\rho_\xi^2}\frac{1}{\sin^2\theta}I_\gamma\otimes H^r_\chi + H_V I_\gamma\otimes I_\chi) \tag{64}$$

Now H^s is divided into two terms

$$H_1^s = \frac{\hbar^2}{2\mu\rho_\xi^2} H_\gamma \otimes I_\chi \tag{65}$$

$$H_2^s = \frac{\hbar^2}{2\mu\rho_\xi^2} \frac{1}{\sin^2\theta} I_\gamma \otimes H_\chi + H_V I_\gamma \otimes I_\chi \tag{66}$$

The first term, H_1^s, is independent of χ, while the second term is dependent of both γ and χ. Since we are interested in only the lowest eigenvalues and eigenfunctions of H^s, and H_1^s is independent of χ, we can expect to get accurate results using only a subeigenspace of H_2^s instead. We solve the eigensystem of H_2^s for each fixed γ_j,

$$H_2^s(\gamma_j)\alpha_k^{\gamma_j} = \lambda_k^{\gamma_j}\alpha_k^{\gamma_j} \quad j = 1, N_\gamma \tag{67}$$

where N_γ is the number of the grid points used in γ and $(\lambda_k^{\gamma_j}, \alpha_k^{\gamma_j})$ is the k-th eigenpair for the given γ_j. Then we drop the eigenvectors with large eigenvalues. The rest of the eigenvectors consist of a nearly complete basis for the lowest eigenvectors of H^s. In our implementation, we sort all the eigenvectors obtained above in ascending order of eigenvalues, and choose only a number of the eigenvectors corresponding to the smallest eigenvalues. After normalization they compose the projection matrix,

$$P = \begin{pmatrix} P_1 & & & \\ & P_2 & & \\ & & \ddots & \\ & & & P_{N_\gamma} \end{pmatrix} \tag{68}$$

where

$$P_i = (\alpha_1^{\gamma_i}, \alpha_2^{\gamma_i}, \ldots, \alpha_{m_{\gamma_i}}^{\gamma_i}) \tag{69}$$

Because P is an orthonormal, nearly complete basis for the lowest eigenvectors, $\overline{\Phi}_{\tau\Lambda}^p(\gamma, \chi; \rho_\xi)$, we have

$$P\widetilde{P}\overline{\Phi}_{\tau\Lambda}^p(\gamma, \chi; \rho_\xi) \approx \overline{\Phi}_{\tau\Lambda}^p(\gamma, \chi; \rho_\xi) \tag{70}$$

Substituting $\overline{\Phi}_{\tau\Lambda}^p(\gamma, \chi; \rho_\xi)$ in (48) and left multiplying $\widetilde{P}$ at its both sides, we get,

$$H^{\text{cut}}\Psi_{\tau\Lambda}^p(\gamma, \chi; \rho_\xi) \approx \mathcal{E}_{\tau\Lambda}^p(\rho_\xi)\Psi_{\tau\Lambda}^p(\gamma, \chi; \rho_\xi) \tag{71}$$

where

$$H^{\text{cut}} = \widetilde{P}HP \tag{72}$$

and

$$\Psi_{\tau\Lambda}^p(\gamma, \chi; \rho_\xi) = \widetilde{P}\overline{\Phi}_{\tau\Lambda}^p(\gamma, \chi; \rho_\xi) \tag{73}$$

We can see that P is a $N_\gamma N_\chi \times N_\chi^{\text{cut}}$ matrix, where

$$N^{\text{cut}} = \sum_{i=1}^{N_\gamma} m_{\gamma_i} \tag{74}$$

so H^{cut} is a $N^{\text{cut}} \times N^{\text{cut}}$ matrix. Its size is much smaller than the size of H^s if N^{cut} is much smaller than $N_\gamma N_\chi$, which is the case if we want only a few eigenvalues. N^{cut} should be as small as possible and it should be decided in the convergence test.

Knowing that H^s is symmetric, we have

$$\widetilde{H}^{\text{cut}} = \widetilde{P}\widetilde{H}^s P = \widetilde{P}H^s P = H^{\text{cut}} \tag{75}$$

Thus H^{cut} is symmetric.

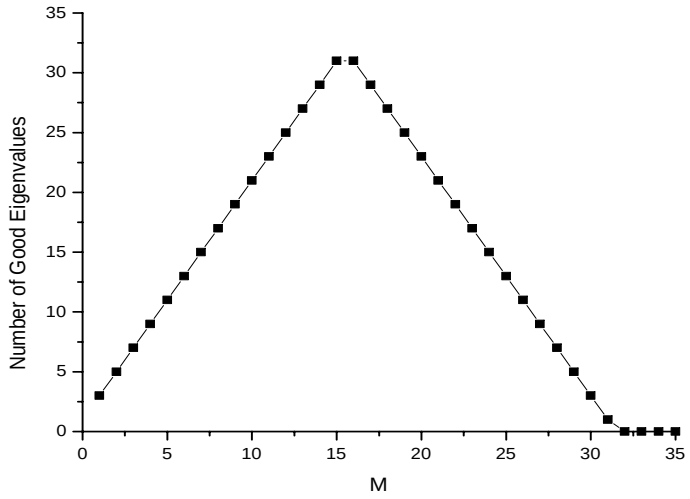

Figure 3: The number of good eigenvalues reaches maximum when $M = N_\chi/2$ ($N_\chi = 32$), where M is the parameter in PDAF $\delta^{(k)}_{p,M}(x)$, and N_χ is the number of gird points in range $(0, 2\pi)$. fig:TestM

4 Numerical Tests

sec:Test Numerical tests are carried out in three aspects. First, we test the and decide the parameter M in PDAF $\delta^{(k)}_{p,M}$. Then we test the H^r_χ with different irreducible representations of varies groups. The accuracy of H^r_γ is tested at last.

4.1 Test of PDAFs

We tested PDAFs using different periodic functions, all of them show the similar results. Here we present only the test with the eigenvalues of H_χ. Using the PDAF matrix defined in (17), we obtain the discrete presentation of H_χ,

$$\begin{aligned} H_{\chi_{ij}} &= -\sum_{k=1}^{N_\chi} D^{(2)}_{ij} \\ &= -\sum_{k=1}^{N_\chi} \delta^{(2)}_{p,M}(\chi_i - \chi_j)\Delta\chi \end{aligned} \tag{76}$$

where N_χ is the number of grid points used in $(0, 2\pi)$, $\Delta\chi = 2\pi/N_\chi$ and $\chi_j = (j - \frac{1}{2})\Delta\chi$. We know that the correct eigenvalues of H_χ should be $0, 1, 1, 4, 4, \cdots, k^2, k^2, \cdots$, so it's easy to check the difference between the computed eigenvalues and the exact ones. We set the criteria of 10^{-6} as the maximum tolerable error, then we can count how many good eigenvalues can be obtained. One typical result is shown in Fig. 3 , in which we set $N_\chi = 32$ and varies M from 1 to 35. One can see that when $M = N_\chi/2$, almost all eigenvalues are good. This suggests the nearly optimal choice of M.

4.2 Test of H^r_χ

Test of H^r_χ are done in all aforementioned irreducible representations of all point groups. All of them give ideal results. Here we present only one typical result computed using C_{2v} group, because only

C_{2v} is used in FH_2 reaction calculation.

Similar to H_χ, we can obtain the PDAF presentation of H^r_χ. Note that C_{2v} has only one-dimensional irreducible representations, so we should use (60) for H^r_χ. We obtain the discrete presentation of H^r_χ as,

$$H_{\chi_{ij}} = -\sum_{k=1}^{N_\chi}\sum_{R}\delta^{(2)}_{p,M}(\chi_i - R\chi_j)\Gamma^{[z]}\Delta\chi \tag{77}$$

Note that the grid scheme is defined in (52). We set $N_\chi = 8$, and the eigenvalues λ_k for each irreducible representations are computed, and $\sqrt{\lambda_k}$ are shown in table 1 for easy comparison. One can see that if we combine the results from all the irreducible representations, we will obtain the (approximate) eigenvalues $0, 1, 1, 4, 4, \cdots, k^2, k^2, \cdots$, which is obtained from H_χ. And we also note that the degenerate eigenvalues in H_χ are no longer degenerate in H^r_χ.

k	A_1	B_1	A_2	B_2
1	0.00000052456066	2.00000000000009	0.99999999999989	1.00000000000007
2	2.00000000000007	3.99999999999997	3.00000000000004	3.00000000000002
3	3.99999999999999	5.99999999999999	5.00000000000000	5.00000000000000
4	5.99999999999999	7.99999999999999	7.00000000000000	7.00000000000000
5	7.99999999999999	10.0000000000000	9.00000000000001	9.00000000000001
6	10.0000000000000	12.0000000000000	11.0000000000000	11.0000000000000
7	12.0000000000000	14.0000000000000	13.0000000000000	13.0000000000000
8	14.0000000000000	22.6274169979695	15.0000000000000	15.0000000000000

Table 1: $\sqrt{\lambda_k}$, square roots of eigenvalues of H^r_χ in irreducible representations of group C_{2v} tbl:eigenHchiC2v

4.3 Test of H^r_γ

H^r_γ in (46) has the same eigenvalues as H_θ in (24). If we rewrite H_θ as

$$H_\theta = -\frac{8}{\sin 2\theta}\frac{\partial}{\partial 2\theta}\sin 2\theta\frac{\partial}{\partial 2\theta} \tag{78}$$

we can see that the eigen-equation of H_θ, (28), is a Legendre differential equation if we let the eigenvalue,

$$\lambda_l = 8l(l+1) \;\; l = 0, 1, ... \tag{79}$$

Thus H^r_γ has eigenvalues of $8l(l+1)$. To evaluate the accuracy of the computed eigenvalue, we define $S_l(\lambda_l)$ as follows,

$$S_l(\lambda_l) = \begin{cases} -\lg|\lambda_l| & \text{l=0,} \\ -\lg\frac{\lambda_l - 8l(l+1)}{8l(l+1)} & l > 0. \end{cases} \tag{80}$$

where λ_l is the l-th computed eigenvalues, and $S_l(\lambda_l)$ gives approximate number of significant digits. Fig. 4 shows the results when we set $N_\gamma = 16, 32, 48$ and 64. One can see that for each N_γ there are about $N_\gamma/3$ of the eigenvalues are of high accuracy. This is accurate enough for the FH_2 calculation, because typically the order of the Hamiltonian matrix is about 1000 but we wants less than 300 eigenvalues.

It is worth to mention that we also tested the non-symmetric form, H_θ, using PDAF presentation. Although we can get as very high accurate results as we get from H_χ or H^r_χ, we still choose the symmetric form, because the non-symmetric matrix will cost too much time and memory to diagonalize. Moreover, if when we add potential, the accuracy the of the non-symmetric form will drop to the accuracy of the H^r_γ.

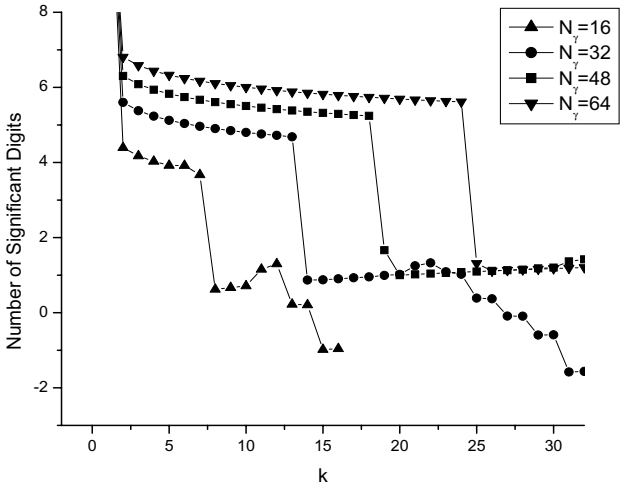

Figure 4: Accuracy (number of significant digits) in eigenvalues of H^r_γ. For all N_γ, the smallest $N_\gamma/3$ eigenvalues are of high accuracy.

fig:AccurHgamma

5 Calculation of FH_2 System

sec:CalcFH2

In this section we report the results of PDAF calculation s of surface functions and the matrix elements, and compare them with the results of the DVR and ABM methods. The system chosen as a nontrivial example is the $F+H_2 \rightarrow HF+H$ reaction; its treatment requires generation of a large basis of surface functions. The potential energy surface (PES) used is the one of Brown et al.[18] commonly called the T5A surface, and we choose the zero of energy to be at the bottom of the asymptotic HF potential wells. This PES has been used in many calculations[1, 19, 5, 14, 20, 21, 22] on this reaction, and plots of the PES and surface functions showing their appearance in APH coordinates have also been published. Arrangement 1 or i(initial) is that of the $F+H_2$ reactants.

The calculations are for $\Lambda = 0$ and even parity ($p = 0$) and include all functions connecting to the even j rotational states of the $F+H_2$ arrangement. Because of the symmetry due to the identical H atoms, this only requires including in the PDAF calculations the A_1 irreducible representation, in which the surface functions are even under reflection about $\chi = 0$.

5.1 Gird Size and Mapping

The grid sizes(the number of grid points),N_χ, N_γ, and $N^{\rm cut}$ are decided in the convergence test. We present only the results here. To reach five significant digits in the lowest 100 eigenvalues for any ρ_ξ,

$$N_\gamma = \lfloor 25.852 + 5.85119\rho_\xi - 0.130102\rho_\xi^2 - 0.0042517 * \rho_\xi^3 \rfloor \quad (81)$$

$$N^{\rm cut} = \lfloor 1428.06 + 29.2007\rho_\xi - 6.37755\rho_\xi^2 - 0.119048 * \rho_\xi^3 \rfloor \quad (82)$$

$$N_\chi = \lfloor 4\pi \max(N_\gamma) \rfloor / h \quad (83)$$

where h is the order of the associated symmetry group. To get the N_χ, we use the maximum of N_γ because it can make N_χ identical for all ρ_ξ, thus make it easy to compute the overlap matrices. And using the maximum N_γ doesn't significantly increase the computation time, because we reduce the

matrix size according to $N^{\rm cut}$, as we discussed in Sec. 3.4 .

Although N_χ's are identical to varies ρ_ξ, N_γ's are not. So before we compute the overlap matrix, we have to map the wave functions to a uniformed grid set to reduce the computation time on the overlap matrix.

Let N_γ^u be the uniformed number of grid points in γ, N_γ is the original number of grid points. Applying (15) to the wave function

$$\begin{aligned}
\Phi^p_{\tau\Lambda}(\gamma_j,\chi;\rho_\xi) &= \sum_{k=1}^{2N_\gamma} \delta_{p,M}(\gamma_j-\gamma_k)\Phi^p_{\tau\Lambda}(\gamma_k,\chi;\rho_\xi)\Delta\gamma \\
&= \sum_{k=1}^{N_\gamma} \left\{\delta_{p,M}(\gamma_j-\gamma_k)\Phi^p_{\tau\Lambda}(\gamma_k,\chi;\rho_\xi) + \delta_{p,M}(\gamma_j-2\pi+\gamma_k)\Phi^p_{\tau\Lambda}(2\pi-\gamma_k,\chi;\rho_\xi)\right\}\Delta\gamma \\
&= \sum_{k=1}^{N_\gamma} \left[\delta_{p,M}(\gamma_j-\gamma_k) + \delta_{p,M}(\gamma_j-2\pi+\gamma_k)\right]\Phi^p_{\tau\Lambda}(\gamma_k,\chi;\rho_\xi)\Delta\gamma \qquad (84)
\end{aligned}$$

where $\Delta\gamma = \pi/N_\gamma$, and γ_j,γ_k represent the coordinates in the above two grid schemes respectively, say,

$$\gamma_j = (j-\frac{1}{2})\Delta\gamma^u \qquad (85)$$

$$\gamma_k = (k-\frac{1}{2})\Delta\gamma \qquad (86)$$

where $\Delta\gamma^u = \pi/N_\gamma^u$

5.2 Eigenvalues

The atomic masses used are:

$$\text{mass of F} = 18.9984032 \text{ a.u.} \qquad (87)$$

$$\text{mass of H} = 1.00782503 \text{ a.u.} \qquad (88)$$

The calculations were performed at five representative ρ values ranging from the smallest to the largest values needed in our reactive scattering calculations[5, 14]. The precise values of ρ chosen have no particular meaning, and some were chosen simply because the convergence of the DVR method had already been studied there.

The results are given in Table 2 through Table 6 for the five values of ρ chosen. In each the energy eigenvalues of the highest ten important or open surface function states are given in eV. The omitted lower eigenvalues always agree even better than those shown. Also shown is $\overline{\mathcal{E}}(n)$, the average of the first n eigenvalues. This gives a convenient measure of the overall agreement of the methods.

5.3 Matrix Elements

The APH surface functions $\Phi^p_{\tau\Lambda}(\gamma,\chi;\rho_\xi)$ are "sector adiabatic"; that it, they change from sector to sector, but are independent of ρ on a sector. Thus, when the APH wave function is substituted into the Schrödinger equation, the resulting exact coupled channel or close coupling equations are of the form[3]

$$\left[\frac{\partial^2}{\partial\rho^2} + \frac{2\mu E}{\hbar^2}\right]\psi^{Jpn}_{\tau\Lambda}(\rho) = \frac{2\mu}{\hbar^2}\sum_{\tau^{\emptyset}A^{\emptyset}} \langle\Phi^{Jp}_{\tau\Lambda}\hat{D}^{Jp}_{\Lambda M}|H_i|\Phi^{Jp}_{\tau^{\emptyset}\Lambda^{\emptyset}}\hat{D}^{Jp}_{\Lambda^{\emptyset}M}\rangle\psi^{Jpn}_{\tau^{\emptyset}\Lambda^{\emptyset}}\rho \qquad (89)$$

τ	PDAF	ABM	DVR	FEM
1	6.9176	6.9177	6.9177	6.9177
2	7.0341	7.0341	7.0341	7.0342
3	7.1299	7.1298	7.1296	7.1299
4	7.3044	7.3042	7.3038	7.3043
5	7.4934	7.4932	7.4927	7.4933
6	7.7007	7.7007	7.7008	7.7009
7	7.9227	7.9219	7.9202	7.9222
8	8.0786	8.0789	8.0786	8.0791
9	8.1548	8.1524	8.1475	8.1529
10	8.2495	8.2502	8.2494	8.2503
$\overline{\mathcal{E}}(10)$	7.5986	7.5983	7.5974	7.5985

Table 2: PDAF, ABM, DVR, and FEM surface function energies $\mathcal{E}_\tau$ and average energies in eV at $\rho = 2.2\ a_0$.

tbl:E2.2

τ	PDAF	ABM	DVR	FEM
11	1.9845	1.9845	1.9845	1.9849
12	1.9975	1.9975	1.9975	1.9979
13	2.0514	2.0515	2.0515	2.0519
14	2.1090	2.1090	2.1090	2.1093
15	2.1275	2.1275	2.1275	2.1281
16	2.1352	2.1352	2.1353	2.1357
17	2.1993	2.1994	2.1994	2.1998
18	2.2578	2.2578	2.2578	2.2584
19	2.2730	2.2730	2.2730	2.2737
20	2.3197	2.3197	2.3197	2.3204
$\overline{\mathcal{E}}(20)$	1.8551	1.8551	1.8551	1.8554

Table 3: PDAF, ABM, DVR, and FEM surface function energies $\mathcal{E}_\tau$ and average energies in eV at $\rho = 3.0375828\ a_0$.

tbl:E3.0

τ	PDAF	ABM	DVR	FEM
91	2.0699	2.0701	2.0701	2.0720
92	2.0721	2.0734	2.0727	2.0760
93	2.0864	2.0896	2.0869	2.0916
94	2.0941	2.0941	2.0943	2.0961
95	2.1087	2.1107	2.1093	2.1132
96	2.1215	2.1232	2.1220	2.1267
97	2.1487	2.1509	2.1495	2.1549
98	2.1643	2.1650	2.1645	2.1672
99	2.1793	2.1806	2.1799	2.1833
100	2.1892	2.1892	2.1893	2.1918
$\overline{\mathcal{E}}(100)$	1.3974	1.3977	1.3975	1.3985

Table 4: PDAF, ABM, DVR, and FEM surface function energies $\mathcal{E}_\tau$ and average energies in eV at $\rho = 4.9747966\ a_0$.

tbl:E4.9

τ	PDAF	ABM	DVR	FEM
91	2.0559	2.0564	2.0569	2.0679
92	2.0749	2.0754	2.0760	2.0928
93	2.0980	2.0981	2.0981	2.1023
94	2.0985	2.0990	2.0994	2.1141
95	2.1098	2.1098	2.1099	2.1148
96	2.1194	2.1196	2.1198	2.1278
97	2.1268	2.1273	2.1278	2.1443
98	2.1538	2.1542	2.1543	2.1537
99	2.1551	2.1551	2.1551	2.1608
100	2.1597	2.1602	2.1608	2.1621
$\overline{\mathcal{E}}(100)$	1.3788	1.3788	1.3790	1.3811

Table 5: PDAF, ABM, DVR, and FEM surface function energies $\mathcal{E}_\tau$ and average energies in eV at $\rho = 7.2989993\ a_0$.

tbl:E7.2

τ	PDAF	ABM	DVR	FEM
91	2.0747	2.0747	2.0748	2.0805
92	2.0774	2.0779	2.0782	2.0863
93	2.0957	2.0964	2.0974	2.1051
94	2.1010	2.1010	2.1009	2.1065
95	2.1153	2.1153	2.1154	2.1233
96	2.1189	2.1194	2.1197	2.1284
97	2.1250	2.1252	2.1253	2.1315
98	2.1461	2.1470	2.1482	2.1541
99	2.1542	2.1545	2.1546	2.1562
100	2.1558	2.1559	2.1560	2.1564
$\overline{\mathcal{E}}(100)$	1.3791	1.3791	1.3792	1.3812

Table 6: PDAF, ABM, DVR, and FEM surface function energies $\mathcal{E}_\tau$ and average energies in eV at $\rho = 9.0a_0$.

tbl:E9.0

The matrix elements are obtained in Reference [3] as,

$$\begin{aligned}
& \langle \Phi^{Jp}_{\tau\Lambda} \hat{D}^{Jp}_{\Lambda M} | H_i | \Phi^{Jp}_{\tau^{\theta}\Lambda^{\theta}} \hat{D}^{Jp}_{\Lambda^{\theta} M} \rangle \\
= & \frac{\rho_{\xi}^2}{\rho^2} \mathcal{E}_{\tau\Lambda}(\rho_{\xi}) \delta_{\tau\tau^{\theta}} \delta_{\Lambda\Lambda^{\theta}} \\
& + \delta_{\Lambda\Lambda^{\theta}} \langle \Phi^{Jp}_{\tau\Lambda} \left| V(\rho,\theta,\chi) - \frac{\rho_{\xi}^2}{\rho^2} V(\rho_{\xi},\theta,\chi) \right| \Phi^{Jp}_{\tau^{\theta}\Lambda} \rangle \\
& + \langle \Phi^{Jp}_{\tau\Lambda} \hat{D}^{Jp}_{\Lambda M} \left| \frac{A-B}{2}(J_x^2 - J_y^2) + T_c \right| \Phi^{Jp}_{\tau^{\theta}\Lambda^{\theta}} \hat{D}^{Jp}_{\Lambda^{\theta} M} \rangle
\end{aligned} \tag{90}$$

where ρ_{ξ}denoted the ξ^{th} hyper radius we sampled from interval $[\rho_{\min}, \rho_{\max}]$. ρ_{ξ} is given by

$$\rho_{\xi} = [\rho_{\min} + (\xi - 1)\Delta\rho_1](1 + \Delta\rho_2)^{\xi - 1} \tag{91}$$

This basis code spaces sector centers logarithmically. Given a sector with sector center ρ_{ξ}, we evaluate matrix elements at three rho values on at

$$\rho_1 = \frac{\rho_{\xi-1} + \rho_{\xi}}{2} \tag{92}$$

$$\rho_2 = \rho_{\xi} \tag{93}$$

$$\rho_3 = \frac{\rho_{\xi} + \rho_{\xi+1}}{2} \tag{94}$$

All the matrix elements in (90) are independent of E, so that they can be calculated once, stored, and used at many scattering energies.

Normalization of the wave functions $\Phi^{p}_{\tau,\Lambda}(\gamma,\chi;\rho_{\xi})$ should be conducted before computation of the matrix elements. The normalization factor N can be calculated in the irreducible representation easily according to (23) as shown below,

$$\begin{aligned}
1 &= N \int_0^{2\pi} d\chi \int_0^{\pi/2} d\theta \sin 2\theta {\Phi^{p}_{\tau\Lambda}}^2(\theta,\chi;\rho_{\xi}) \\
&= N \int_0^{2\pi} d\chi \int_0^{\pi} d\gamma \frac{\pi}{4} \sin\gamma \sin 2\theta {\Phi^{p}_{\tau\Lambda}}^2(\gamma,\chi;\rho_{\xi}) \\
&= N \sum_{i=1}^{hN_{\chi}} \sum_{j=1}^{N_{\gamma}} \Delta\chi\Delta\gamma \frac{\pi}{4} \sin\gamma_j \sin 2\theta(\gamma_j) {\Phi^{p}_{\tau\Lambda}}^2(\gamma_j,\chi_i;\rho_{\xi}) \\
&= N \sum_{i=1}^{N_{\chi}} \sum_{j=1}^{N_{\gamma}} \sum_{R} \Delta\chi\Delta\gamma \frac{\pi}{4} \sin\gamma_j \sin 2\theta(\gamma_j) \Phi^{p}_{\tau\Lambda}(\gamma_j, R^{-1}\chi_i;\rho_{\xi}) \Phi^{p}_{\tau\Lambda}(\gamma_j, R^{-1}\chi_i;\rho_{\xi}) \\
&= N \sum_{i=1}^{N_{\chi}} \sum_{j=1}^{N_{\gamma}} \sum_{R} \Delta\chi\Delta\gamma \frac{\pi}{4} \sin\gamma_j \sin 2\theta(\gamma_j) {\Gamma^{[z]}}^2(R) {\Phi^{p}_{\tau\Lambda}}^2(\gamma_j,\chi_i;\rho_{\xi}) \\
&= hN \sum_{i=1}^{N_{\chi}} \sum_{j=1}^{N_{\gamma}} \Delta\chi\Delta\gamma \frac{\pi}{4} \sin\gamma_j \sin 2\theta(\gamma_j) {\Phi^{p}_{\tau\Lambda}}^2(\gamma_j,\chi_i;\rho_{\xi})
\end{aligned}$$

Thus

$$N = \left\{ \frac{1}{4} h\pi\Delta\chi\Delta\gamma \sum_{i=1}^{N_{\chi}} \sum_{j=1}^{N_{\gamma}} \sin\gamma_j \sin 2\theta(\gamma_j) {\Phi^{p}_{\tau\Lambda}}^2(\gamma_j,\chi_i;\rho_{\xi}) \right\}^{-\frac{1}{2}} \tag{95}$$

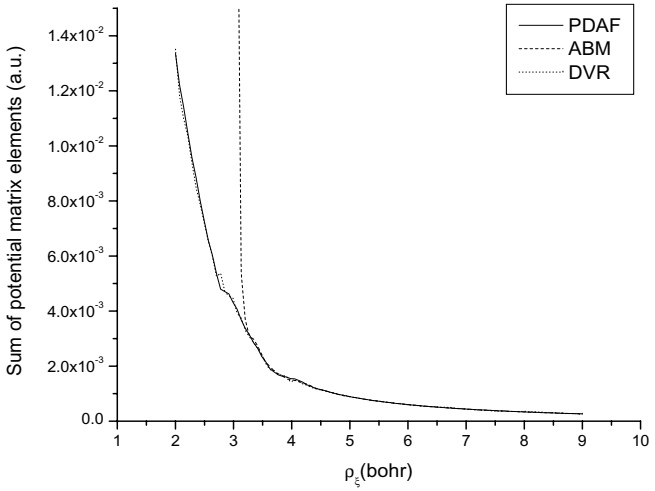

Figure 5: Comparison of the Sum of potential matrix elements using PDAF, ABM and DVR fig:SPotmat

Assuming $\Phi^p_{\tau\Lambda}(\gamma,\chi;\rho_\xi)$ is normalized, we can start computing the matrix elements. The first term on the right-hand side of (90) is just a local internal energy which together with the E term on the left-hand side of (89) makes a local wave number.

The second term of (89) is often called potential matrix elements. It is small on the sector and can be evaluated with the same quadratures used in getting the surface functions. Similar to the way to obtain the normalization factor, we can get the formula of the potential matrix elements,

$$\begin{aligned}
&\langle \Phi^{Jp}_{\tau\Lambda}(\rho_\xi) \mid V(\rho) - \frac{\rho_\xi^2}{\rho^2} V(\rho_\xi) \mid \Phi^{Jp}_{\tau^{\prime}\Lambda}(\rho_\xi)\rangle \\
&= \frac{1}{4} h\pi\Delta\chi\Delta\gamma \sum_{i=1}^{N_\chi}\sum_{j=1}^{N_\gamma} \sin\gamma_j \sin 2\theta(\gamma_j) \times \\
&\Phi^p_{\tau\Lambda}(\gamma_j,\chi_i;\rho_\xi) \left[V(\rho) - \frac{\rho_\xi^2}{\rho^2} V(\rho_\xi) \right] \Phi^p_{\tau^{\prime}\Lambda}(\gamma_j,\chi_i;\rho_\xi)
\end{aligned} \tag{96}$$

The Coriolis term can be simplified as

$$\begin{aligned}
&\langle \Phi^{Jp}_{\tau\Lambda} \hat{D}^{Jp}_{\Lambda M} | T_c | \Phi^{Jp}_{\tau^{\prime}\Lambda^{\prime}} \hat{D}^{Jp}_{\Lambda^{\prime} M} \rangle \\
= \;& \frac{-\hbar^2}{2\mu\rho^2} \left\langle \Phi^p_{\tau\Lambda} \left| \frac{\cos\theta}{\sin^2\theta} \frac{\partial}{\partial\chi} \right| \Phi^p_{\tau^{\prime}\Lambda^{\prime}} \right\rangle \\
&\times [(1+\delta_{\Lambda 0})(1+\delta_{\Lambda^{\prime} 0})]^{-1/2} \\
&\times [\lambda_+(J,\Lambda)\delta_{\Lambda^{\prime},\Lambda+1} - \lambda_-(J,\Lambda)\delta_{\Lambda^{\prime},\Lambda-1} \\
&+\lambda_-(J,\Lambda)(-1)^{J+\Lambda+p}\delta_{\Lambda,1-\Lambda}]
\end{aligned} \tag{97}$$

where

$$\lambda_\pm(J,\Lambda) = [(J\pm\Lambda+1)(J\mp\Lambda)]^{\frac{1}{2}} \tag{98}$$

and

$$\left\langle \Phi^p_{\tau\Lambda} \left| \frac{\cos\theta}{\sin^2\theta}\frac{\partial}{\partial\chi} \right| \Phi^p_{\tau^0\Lambda^0} \right\rangle$$
$$= \frac{1}{2}h\pi\Delta\chi^2\Delta\gamma \sum_{i=1}^{N_\chi}\sum_{j=1}^{N_\gamma}\sum_{k=1}^{N_\chi} \sin\gamma_j \frac{\cos^2\theta(\gamma_j)}{\sin\theta(\gamma_j)} \times$$
$$\Phi^p_{\tau\Lambda}(\gamma_j,\chi_i;\rho_\xi)\delta^{(1)}_{p,M}(\chi_i-\chi_k)\Phi^p_{\tau^0\Lambda^0}(\gamma_j,\chi_k;\rho_\xi) \tag{99}$$

It should be noted that the last term in the bracket can only be nonzero for $\Lambda = 0$ or 1 and also that because the ρ dependence of the operator factors out, the matrix elements over the $\Phi^p_{\tau\Lambda}(\gamma,\chi;\rho_\xi)$ only need be evaluated once on each sector. They are readily evaluated using the PDAF $\Phi^p_{\tau\Lambda}(\gamma,\chi;\rho_\xi)$ and their quadrature points as the PDAF code generates the derivatives of $\Phi^p_{\tau\Lambda}(\gamma,\chi;\rho_\xi)$ directly.

The asymmetric top terms of (90) can be explicitly written as

$$\begin{aligned}
&\langle\tau\Lambda|\frac{1}{2}(A-B)(J_x^2-J_y^2)|\tau'\Lambda'\rangle \\
= \;& \frac{1}{4}\hbar^2\langle\Phi^p_{\tau\Lambda}|A-B|\Phi^p_{\tau^0\Lambda^0}\rangle[(1+\delta_{\Lambda 0})(1+\delta\Lambda' 0)]^{-1/2} \\
&\times[\lambda_+(J,\Lambda)\lambda_+(J,\Lambda+1)\delta_{\Lambda^0,\Lambda+2} \\
&+\lambda_-(J,\Lambda)\lambda_-(J,\Lambda-1)\delta_{\Lambda^0,\Lambda-2} \\
&+(-1)^{J+\Lambda+p}\lambda_-(J,\Lambda)\lambda_-(J,\Lambda-1)\delta_{\Lambda^0,2-\Lambda}]
\end{aligned} \tag{100}$$

where

$$A = \frac{1}{\mu\rho_\xi^2(1+\sin^2\theta)} \tag{101}$$
$$B = \frac{1}{2\mu\rho_\xi^2\sin^2\theta} \tag{102}$$

$$\langle\Phi^p_{\tau\Lambda}|A-B|\Phi^p_{\tau^0\Lambda^0}\rangle$$
$$= \frac{1}{4}h\pi\Delta\chi\Delta\gamma\sum_{i=1}^{N_\chi}\sum_{j=1}^{N_\gamma}\sin\gamma_j\sin 2\theta(\gamma_j)\times$$
$$\Phi^p_{\tau\Lambda}(\gamma_j,\chi_i;\rho_\xi)(A-B)\Phi^p_{\tau^0\Lambda^0}(\gamma_j,\chi_i;\rho_\xi) \tag{103}$$

The third term in the bracket is always zero if $|\Lambda-\Lambda'|>2$, and the ρ dependence of $A-B$ again factors out, giving the same simplifications and allowing the evaluation of the integrals by the same methods as for the Coriolis terms.

At the boundaries between sectors, the R matrix is transformed by an orthogonal transformation, which requires calculation of the overlap matrix elements. The formula of the overlap matrix elements is given by ,

$$\langle\Phi^{Jp}_{\tau\Lambda}(\rho_\xi)\mid\Phi^{Jp}_{\tau^0\Lambda}(\rho_{\xi^0})\rangle$$
$$= \frac{1}{4}h\pi\Delta\chi\Delta\gamma^u\sum_{i=1}^{N_\chi}\sum_{j=1}^{N_\gamma}\frac{\pi}{4}\sin\gamma_j\sin 2\theta(\gamma_j)\times$$
$$\Phi^{Jp}_{\tau\Lambda}(\gamma_j,\chi_i;\rho_\xi)\Phi^{Jp}_{\tau^0\Lambda}(\gamma_j,\chi_i\rho_{\xi^0}) \tag{104}$$

To compare the efficency, we the PDAF, DVR, ABM, and FEM programs on the same computer (PIII 866MHz), computing eigenvalues, potential matrix elements, and overlap matrices at 100 ρ_ξ's.

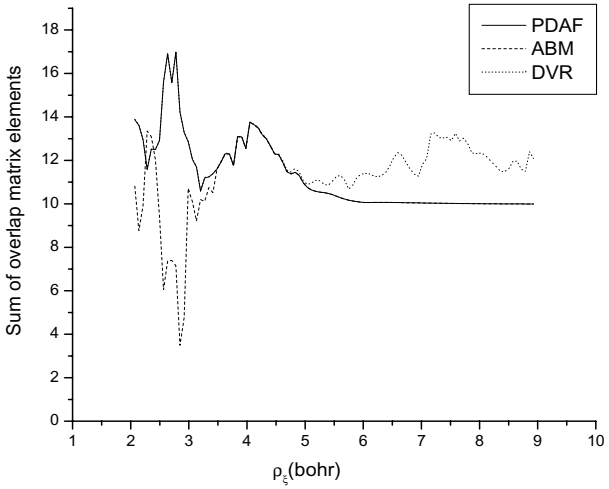

Figure 6: Comparison of the Sum of the overlap matrix elements using PDAF, ABM and DVR. fig:SOverlap

ρ_ξ starts from 2.0 a_0 and ends at 9.0 a_0 and evenly spaced in between. The computation times (CPU time) are shown in Fig. 7 . FEM method takes much more time than the others, thus we do not include it in Fig. 7 . We can see PDAF method is much faster than DVR at most range of ρ_ξ. If ρ_ξ is very small (less than 2.2 a_0), DVR is the most efficient method. Although ABM works slightly faster than PDAF method, but it turns out that ABM diverges when ρ_ξ is small.

We compare only the potential matrix elements and the overlap matrix elements here. Those matrix elements are computed by ABM, DVR and PDAF. The comparison of the potential matrix elements is shown in Fig. 5 , one can see that all the three methods agree with each other very well when $\rho > 3.3a_0$. However, when $\rho < 3.3$, the result of ABM digresses from PDAF and DVR very much. The comparison of the overlap matrix elements is shown in Fig. 6 . One can see clearly from the figure that PDAF gives very close results to DVR at small ρ ($rho < 3.4a_0$), and it also agrees with ABM very well at large ρ ($rho > 4.4a_0$). ABM gives very different results from PDAF and DVR at small ρ, and DVR gives very different results from PDAF and ABM at large ρ. We know that ABM works very accurate at large ρ region and DVR at small ρ region, thus the comparisons tell that PDAF works accurate at both small ρ and large ρ.

6 Conclusion

c:Conclusion

In this paper we have presented a peridoic distributed approximating function (PDAF) method for calculating the surface function basis needed in hyperspherical formulations of reactive scattering theory. PDAF functions are intoduced and shown capable of providing an accurate, efficient representation of the derivative operators.

Test calculations on the $F + H_2$ system with the T5A PES comparing the PDAF, ABM, DVR and FEM methods showed that the FEM is always the least efficient of the four, ABM is the most efficient method for large ρ but is not accurate at small ρ. On the other hand, DVR is the most efficient method for small ρ but is not accurate for large ρ. PDAF is compariablely efficient in both large ρ as ABM and small ρ as DVR and it is accurate for all both small ρ and large ρ. As a result, PDAF is the best method for surface function calcultaions in hyperspherical reactive scattering calculations.

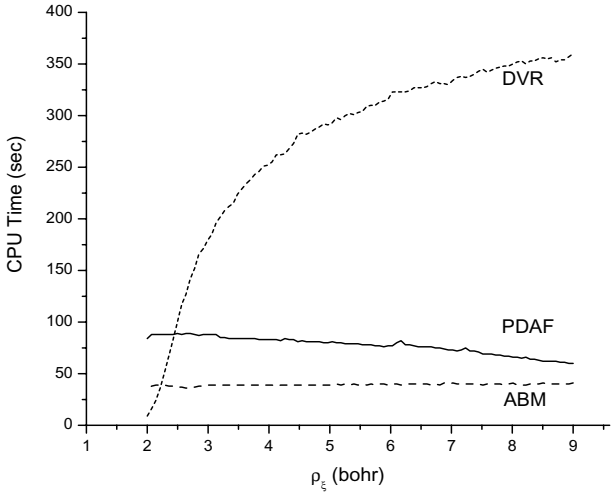

Figure 7: CPU Time of PDAF, DVR and ABM

fig:Time-Rho

7 Acknowledgements

We would like to thank the National Science Foundation NSF CHE-9710383 and NSF PHY-0100704 for support. One of us (GAP) would also like to thank the members of Group T-12 at the Los Alamos National Laboratory (LANL) for their helpfulness and hospitality extended during summer visits.

A H^r_χ is symmetric

app:symproof

$$H^r_\chi(\chi_i,\chi_j) = \sum_R H_\chi(\chi_i, R\chi_j)\Gamma^{[\tau]*}(R) \tag{105}$$

To prove that H^r_χ is symmetric, it is sufficient to show

$$H^r_{\chi_{\kappa,\kappa^0}}(\chi_i,\chi_j) = H^r_{\chi_{\kappa^0,\kappa}}(\chi_j,\chi_i) \tag{106}$$

eq:sym

where

$$H^r_{\chi_{\kappa,\kappa^0}}(\chi_i,\chi_j) = \sum_R H_\chi(\chi_i, R\chi_j)\Gamma^{[z]*}_{\kappa,\kappa^0}(R) \tag{107}$$

eq:Hele

We know that H_χ is symmetric, so

$$\begin{aligned} H^r_{\chi_{\kappa^\theta,\kappa}}(\chi_j,\chi_i) &= \sum_R H_\chi(\chi_j, R\chi_i)\Gamma^{[z]*}_{\kappa^\theta,\kappa}(R) \\ &= \sum_R H_\chi(R\chi_i,\chi_j)\Gamma^{[z]*}_{\kappa^\theta,\kappa}(R) \\ &= \sum_R H_\chi(R^{-1}\chi_i,\chi_j)\Gamma^{[z]*}_{\kappa^\theta,\kappa}(R^{-1}) \\ &= \sum_R H_\chi(R^{-1}\chi_i,\chi_j)\Gamma^{[z]*-1}_{\kappa^\theta,\kappa}(R) \\ &= \sum_R H_\chi(R^{-1}\chi_i,\chi_j)\Gamma^{[z]*\dagger}_{\kappa^\theta,\kappa}(R) \\ &= \sum_R H_\chi(R^{-1}\chi_i,\chi_j)\Gamma^{[z]}_{\kappa,\kappa^\theta}(R) \end{aligned} \tag{108}$$

Because $H_\chi(\chi_i,\chi_j)$ ($DAF^{(2)}(\chi_i-\chi_j)$) is decided by $|\chi_i-\chi_j|$, and R is a length-conservative operation, we have

$$\begin{aligned} H_\chi(R^{-1}\chi_j,\chi_i) &= H_\chi(R^{-1}\chi_j,\chi_i) \\ &= H_\chi(RR^{-1}\chi_j,R\chi_i) \\ &= H_\chi(\chi_j,R\chi_i) \end{aligned} \tag{109}$$

Combination of (108) and (109) gives

$$H^r_{\chi_{\kappa,\kappa^\theta}}(\chi_i,\chi_j) = \sum_R H_\chi(\chi_i,R\chi_j)\Gamma^{[z]}_{\kappa,\kappa^\theta}(R) \tag{110}$$

So if $\Gamma^{[z]}$ is real, (106) is true, say, if $\Gamma^{[z]}$ is real, H^r_χ is symmetric.

B Irreducible representations of group C_2, C_{2v} and C_{6v}

app:group

The irreducible representation matrices for some point groups frequently used in APH Surface function computation are given in Table 7 , Table 8 and Table 9 . The first column in each table is the names of the irreducible representations. The second row gives the transformation when a symmetry operation R acts on χ. Parity p is also given in each table.

C_2	E	C_2	p
$R\chi$	χ	$\pi+\chi$	
A	1	1	0
B	1	-1	1

tbl:C2

Table 7: Irreducible representations of group C_2

References

Launay1991

[1] J. M. Launay and M. LeDourneuf, Chem. Phys. Lett. 169, 473 (1990); J. M. Launay, Theor. Chim. Acta 79, 183 (1991).

Lepetit1991

[2] B. Lepetit and J. M. Launay, J. Chem. Phys. 95, 5159 (1991).

ckParker1987

[3] R. T. Pack, G. A. Parker, J. Chem. Phys. 87, 3888 (1987).

C_{2v}	E	C_2	σ_v	σ'_v	p
$R\chi$	χ	$\pi+\chi$	$2\pi-\chi$	$\pi-\chi$	
A_1	1	1	1	1	0
A_2	1	1	-1	1	0
B_1	1	-1	1	-1	1
B_2	1	-1	-1	1	1

Table 8: Irreducible representations of group C_{2v}

tbl:C2v

C_{6v}	E	C_6	C_6^5	C_3	C_3^2	C_2	p
$R\chi$	χ	$\frac{\pi}{3}+\chi$	$\frac{5\pi}{3}+\chi$	$\frac{2\pi}{3}+\chi$	$\frac{4\pi}{3}+\chi$	$\pi+\chi$	
A_1	1	1	1	1	1	1	0
A_2	1	1	1	1	1	1	0
B_1	1	-1	-1	1	1	-1	1
B_2	1	-1	-1	1	1	-1	1
E_1	$\begin{pmatrix}1&0\\0&1\end{pmatrix}$	$\begin{pmatrix}\frac{1}{2}&-\frac{\sqrt{3}}{2}\\\frac{\sqrt{3}}{2}&\frac{1}{2}\end{pmatrix}$	$\begin{pmatrix}\frac{1}{2}&\frac{\sqrt{3}}{2}\\-\frac{\sqrt{3}}{2}&\frac{1}{2}\end{pmatrix}$	$\begin{pmatrix}-\frac{1}{2}&-\frac{\sqrt{3}}{2}\\\frac{\sqrt{3}}{2}&-\frac{1}{2}\end{pmatrix}$	$\begin{pmatrix}-\frac{1}{2}&\frac{\sqrt{3}}{2}\\-\frac{\sqrt{3}}{2}&-\frac{1}{2}\end{pmatrix}$	$\begin{pmatrix}-1&0\\0&-1\end{pmatrix}$	1
E_2	$\begin{pmatrix}1&0\\0&1\end{pmatrix}$	$\begin{pmatrix}-\frac{1}{2}&-\frac{\sqrt{3}}{2}\\\frac{\sqrt{3}}{2}&-\frac{1}{2}\end{pmatrix}$	$\begin{pmatrix}-\frac{1}{2}&\frac{\sqrt{3}}{2}\\-\frac{\sqrt{3}}{2}&-\frac{1}{2}\end{pmatrix}$	$\begin{pmatrix}-\frac{1}{2}&\frac{\sqrt{3}}{2}\\-\frac{\sqrt{3}}{2}&-\frac{1}{2}\end{pmatrix}$	$\begin{pmatrix}-\frac{1}{2}&-\frac{\sqrt{3}}{2}\\\frac{\sqrt{3}}{2}&-\frac{1}{2}\end{pmatrix}$	$\begin{pmatrix}1&0\\0&1\end{pmatrix}$	0
R	σ_v	σ'_v	σ''_v	σ_d	σ'_d	σ''_d	p
$R\chi$	$2\pi-\chi$	$\frac{2\pi}{3}-\chi$	$\frac{4\pi}{3}-\chi$	$\frac{\pi}{3}-\chi$	$\pi-\chi$	$\frac{5\pi}{3}-\chi$	
A_1	1	1	1	1	1	1	0
A_2	-1	-1	-1	-1	-1	-1	0
B_1	1	1	1	-1	-1	-1	1
B_2	-1	-1	-1	1	1	1	1
E_1	$\begin{pmatrix}1&0\\0&-1\end{pmatrix}$	$\begin{pmatrix}-\frac{1}{2}&\frac{\sqrt{3}}{2}\\\frac{\sqrt{3}}{2}&\frac{1}{2}\end{pmatrix}$	$\begin{pmatrix}-\frac{1}{2}&-\frac{\sqrt{3}}{2}\\-\frac{\sqrt{3}}{2}&\frac{1}{2}\end{pmatrix}$	$\begin{pmatrix}\frac{1}{2}&\frac{\sqrt{3}}{2}\\\frac{\sqrt{3}}{2}&-\frac{1}{2}\end{pmatrix}$	$\begin{pmatrix}-1&0\\0&1\end{pmatrix}$	$\begin{pmatrix}\frac{1}{2}&-\frac{\sqrt{3}}{2}\\-\frac{\sqrt{3}}{2}&-\frac{1}{2}\end{pmatrix}$	1
E_2	$\begin{pmatrix}1&0\\0&-1\end{pmatrix}$	$\begin{pmatrix}-\frac{1}{2}&-\frac{\sqrt{3}}{2}\\-\frac{\sqrt{3}}{2}&\frac{1}{2}\end{pmatrix}$	$\begin{pmatrix}-\frac{1}{2}&\frac{\sqrt{3}}{2}\\\frac{\sqrt{3}}{2}&\frac{1}{2}\end{pmatrix}$	$\begin{pmatrix}-\frac{1}{2}&\frac{\sqrt{3}}{2}\\\frac{\sqrt{3}}{2}&\frac{1}{2}\end{pmatrix}$	$\begin{pmatrix}1&0\\0&-1\end{pmatrix}$	$\begin{pmatrix}-\frac{1}{2}&-\frac{\sqrt{3}}{2}\\-\frac{\sqrt{3}}{2}&\frac{1}{2}\end{pmatrix}$	0

Table 9: Irreducible representations of group C_{6v}

tbl:C6v

ckParker1989 [4] R. T. Pack, G. A. Parker, J. Chem. Phys. 90, 3551 (1989).

Bacic1990 [5] Z. Bačić, J. D. Kress, G. A. Parker, and R. T Pack, J. Chem. Phys. 92, 2344 (1990).

Kress1990 [6] J. D. Kress, Z. Bačić, G. A. Parker, and R. T Pack, J. Chem. Phys. 94, 8055 (1990).

Launay1989 [7] J. M. Launay and M. LeDourneuf, Chem. Phys. Lett. 163, 178 (1989).

nderberg1989 [8] J. Linderberg, S. B. Padkjaer, Y. Ohrn, and B. Vessal, J. Chem. Phys. 90, 6254 (1989).

ppermann1989 [9] A. Kuppermann and P. G. Hipes, J. Chem. Phys. 84, 5962 (1986); S. A. Cucaro, P. G. Hipes, and A. Kuppermann, Chem. Phys. Lett. 154, 155(1989), 157, 440 (1989).

Lagana1991 [10] (a) A. Laganà, R. T. Pack, and G. A. Parker, Faraday Discuss. Chem. Soc. 84, 409 (1987); (b) 91, 386 (1991).

Parker1989 [11] G. A. Parker, R. T. Pack, A. Laganà, B. J. Archer, J. D. Kress,a and Z. Bačić, in textit-Super Computer Algorithms for Reactivity, Dynamics and Kinetics of Small Molecules, edited by A. Laganà (Kluwer, Holland, 1989), p. 105.

Iyengar1999 [12] S. S. Iyengar, G. A. Parker, D. J. Kouri, D. K. Hoffman, J. Chem. Phys. 110, 10283 (1999).

WithinDVR [13] See Ref. [5] and therein.

Kress1989 [14] J. D. Kress, Z. Bačić, G. A. Parker, and R. T Pack, Chem. Phys. Lett. 157, 484 (1989).

Kress1990A [15] J. D. Kress, R. T. Pack, G. A. Parker, Chem. Phys. Lett. 170, 306 (1990).

Kress1991 [16] J. D. Kress, Chem. Phys. Lett. 179, 510 (1991).

lniewicz1989 [17] L. Wolniewicz, J. Chem. Phys. 90, 371 (1989);

FH2_T5A [18] F. B. Brown, R. Steckler, D. W. Schwenke, D. G. Truhlar, and B. C. Garrett, J. Chem. Phys. 82, 188 (1985); R. Steckler, D. G. Truhlar, and B. C. Garrett, ibid. 82, 5499 (1985).

Zhang1991 [19] J. Z. H. Zhang, Chem. Phys. Lett. 181, 63 (1991).

Yu1989 [20] C. H. Yu, D. J. Kouri, M. Zhao, D. G. Truhlar, and D. W, Schwenke, Chem. Phys. Lett. 157, 491 (1989); Int. J. Quantum Chem. Symp. 23, 45 (1989).

lopoulos1990 [21] D. E. Manolopoulos, M. D'Mello, and R. E. Wyatt, J. Chem. Phys. 93, 403 (1990).

euhauser1990 [22] D. Neuhauser, M. Baer, R. S. Judson, and D. J. Kouri, Chem. Phys. Lett. 169, 372 (1990); D. Neuhauser, R. S. Judson, R. L. Jaffe, M. Baer, and D. J. Kouri, ibid. 176, 546 (1991).

issbluth1978 [23] M. Weissbluth, Atoms and Molecules, Academic Press, INC. (London) Ltd, 1978.